Synthesis and Structure−Activity Relationships of a New Model of Arylpiperazines. 2.[1] Three-Dimensional Quantitative Structure−Activity Relationships of Hydantoin−Phenylpiperazine Derivatives with Affinity for 5-HT_{1A} and α_1 Receptors. A Comparison of CoMFA Models[2]

María L. López-Rodríguez,*,† Mª Luisa Rosado,† Bellinda Benhamú,† Mª José Morcillo,‡ Esther Fernández,† and Klaus-Jürgen Schaper§

Departamento de Química Orgánica I, Facultad de Ciencias Químicas, Universidad Complutense, Ciudad Universitaria s/n, 28040 Madrid, Spain, Facultad de Ciencias, Universidad Nacional de Educación a Distancia, 28040 Madrid, Spain, and Borstel Research Center, D-23845 Borstel, Germany

Received October 25, 1996[⊗]

A series of 48 bicyclohydantoin−phenylpiperazines (**1**−**4**) with affinity for 5-HT_{1A} and α_1 receptors was subjected to three-dimensional quantitative structure−affinity relationship analysis using comparative molecular field analysis (CoMFA), in order to get insight into the structural requirements that are responsible for 5-HT_{1A}/α_1 selectivity. Good models (high cross-validation correlations and predictive power) were obtained for 5-HT_{1A} and α_1 receptors. The resulting 3D-QSAR models rationalize steric and electrostatic factors which modulate binding to 5-HT_{1A} and α_1 receptors. A comparison of these models gives an additional understanding for 5-HT_{1A}/α_1 selectivity: (a) Substitution at the *ortho* position by a group with negative potential is favorable to affinity for both receptors. (b) The *meta* position seems to be implicated in 5-HT_{1A}/α_1 selectivity. While the 5-HT_{1A} receptor is able to accommodate bulky substituents in the region of its active site, the steric requirements of the α_1 receptor are more restricted (optimum volume of substituent 11−25 Å^3). (c) For both receptors the *para* position represents a region where the volume accessible by the ligands is limited. (d) The hydantoin moiety and the side chain length seem to modulate not only the affinity but also 5-HT_{1A}/α_1 selectivity. The 3D-QSAR models reveal an useful predictive information for the design of new selective ligands.

Introduction

Many endogenous substances such as some hormones and neurotransmitters mediate their intracellular effects through signal transduction pathways that involve G-protein-coupled receptor. The cloning of some of these receptors has revealed their related structures, whose most representative common feature is the presence of seven transmembrane domains constituted by α-helices of 20−25 hydrophobic amino acids.[3−5] The α_1 adrenoceptor and the serotonin 5-HT_{1A} receptor are representative members of this receptor superfamily. In spite of their different pharmacology, they show some common features in their binding sites. As a consequence of such similarities some synthetic ligands (*e.g.* long-chain arylpiperazines like NAN-190 and related compounds[6,7]) bind at both receptors. This peculiarity was also shown by some of the new hydantoin−phenylpiperazine derivatives (**1**−**4**) we have recently reported.[1,8] The affinity of the phenylpiperazine derivatives for both receptors has been attributed to interactions of their aromatic moiety and the N4 of the piperazine ring with the active sites.[9−12]

Here we report a study that applies CoMFA[13,14] methodology to rationalize the relationships between new hydantoin−phenylpiperazine structures (**1**−**4**) and their binding-affinity data at 5-HT_{1A} and α_1 receptors. This data set is used to derive CoMFA models that describe the steric and electrostatic requirements for recognition forces characterizing 5-HT_{1A} and α_1 receptor sites. Our aim is to get insight into the structural factors that are responsible for 5-HT_{1A}/α_1 selectivity, in order to design new ligands with high selectivity for the 5-HT_{1A} receptor.

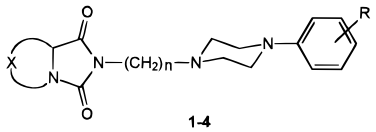

1-4

X=-$(CH_2)_3$-, -$(CH_2)_4$-
n=1, 2, 3, 4
R=H, *o*-OCH_3, *m*-Cl, *m*-CF_3, *p*-F, *p*-NO_2

Materials and Methods

Biological Activities. The compounds were evaluated for *in vitro* 5-HT_{1A} and α_1 receptor affinity by radioligand binding assays. All values have been obtained in rat cerebral cortex membranes with [^{3}H]-8-OH-DPAT and [^{3}H]prazosin as the specific radioligands. The compounds were first tested at the fixed dose of 10^{-6} M, and for those that in this prescreening process presented high activity (displacement of the radioligand ≥55%), the dose−response curves were calculated. However, for the members of the series showing low activity (displacement <55%) the binding constants were not determined. Nevertheless, inactive compounds of a drug series allow the activity scale to be expanded. Obviously a broad range of activity data facilitates the recognition of QSAR relationships. The evaluation of the IC_{50} values for the compounds where only one point of the curve was available was performed by the application of a method,[15] which consists in a simultaneous nonlinear regression analysis of all dose−response curves (DRCs) of the drug series using eq 1.

$$\%SU = 100(1 - C_i^b/(IC_{50j}^b + C_i^b)) \quad (1)$$

† Departamento de Química Orgánica I, Universidad Complutense.
‡ Universidad Nacional de Educación a Distancia.
§ Borstel Research Center.
⊗ Abstract published in *Advance ACS Abstracts,* April 1, 1997.

S0022-2623(96)00744-3 CCC: $14.00

where SU is the specific union of radioligand; *b* is the slope; *i* = 1...*n* (measurements); j: 1...m (number of compounds).

This analysis is performed under the assumption that all derivatives present the same mechanism of action within the given test model (*i.e.* parallel DRCs, identical Hill coeficients/slopes). This approach requires that complete DRCs (≥3 data pairs) are available for some analogs. Missing IC_{50} values are obtained from "fragmentary" DRCs by a computational parallel shift of complete DRCs. IC_{50} values were converted to pK_i values (Tables 1 and 5) using the Cheng−Prusoff equation.[16]

Molecular Modeling and Alignment Rules. The entire set of phenylpiperazine analogs was built *de novo* using the SKETCH option in SYBYL 6.0[17] and fully geometry optimized using the standard TRIPOS molecular mechanics force field, with a 0.001 kcal/mol energy gradient convergence criterion and a distance-dependent dielectric constant. The asymmetric atom was arbitrarily oriented in the *R* configuration. A systematic conformational search was performed on the rotable bonds using an increment at 10° in the SYBYL SEARCH module; MAXIMIN2 steric energies were used to identify low-energy conformations. While it is recognized that low-energy conformations may not necessarily be adopted in the drug−receptor complex, the use of a reasonable low-energy conformation in the alignment is a useful starting point for statistical comparisons of flexible structures within the SYBYL CoMFA module.

The most crucial variable in CoMFA is the positioning of the molecules within a fixed lattice. The best results were obtained when the common pharmacophore portions of all the molecules, comprising the phenylpiperazine moieties, were aligned by a least-squares fit on the following common atoms: (a) the centroid of the aromatic moiety; (b) the N1 and N4 of the phenylpiperazine moiety; and (c) the chain carbon atom adjacent to the N4. This choice of atoms produces a reasonable overlap of the hydantoin substructures, and at the same time allows the best superimposition of the phenylpiperazine moieties.

In order to obtain the best superimposition of the hydantoin moiety in each subfamily of compounds (*n* = 1, 2, 3, and 4), all members of the subfamily were superimposed using the unsubstituted derivative (R = H) with X = $-(CH_2)_3-$ as the template molecule. They were aligned *via* root mean square (RMS) fit of (a) the carbonyl groups of the hydantoin moiety, (b) both hydantoinic nitrogens, (c) the centroid of the pyrrolidine and piperidine ring of the hydantoin substructure, and (d) the common pharmacophore portions. The molecules were aligned initially *via* RMS fit, followed by field fit optimization to the template molecule. Field fitting sometimes forced the molecules into high-energy conformations, in order to obtain maximal similarity between the steric and electrostatic fields of the template and the test molecules. The resulting structures were subsequently reoptimized without the field fit option to allow relaxation of the molecule around the torsion angle.

Low-energy conformers of the variously substituted molecules at the *ortho*, *meta*, and *para* positions of the phenyl ring were chosen for optimal overlap with one another, under the assumption that the substituents at the *ortho* and *meta* positions always occupy the same cavity in the receptor. On these basis all of the *ortho* and *meta* substituents of the phenyl ring were oriented in the same direction. In our experience, CoMFA fails to find a significant correlation if such an approach is not used.

CoMFA Method. The comparative molecular field analysis (CoMFA) was performed using the QSAR option of SYBYL version 6.0 on a Silicon Graphics 4D/25 Personal Iris workstation. The partial atomic charges used in CoMFA were computed using the AM1[18] semiempirical method available in the MOPAC program. Single-point calculations were performed on the geometries previously optimized with SYBYL/MAXIMIN2.

The steric and electrostatic probe−ligand interaction energies (kcal/mol) were calculated with Lennard−Jones and Coulomb potential functions of the Tripos force field using an sp^3 carbon probe carrying a charge of +1.0. The best results were obtained when the steric and electrostatic energies were truncated at 15 and 10 kcal/mol, respectively. The grid used in the CoMFA study had a resolution of 2.0 Å and extended beyond the molecular dimensions by 4.0 Å in all directions. The steric and electrostatic fields were subjected to scaling in order to assign them the same weight (the command "scaling CoMFA_std" was used).

The QSAR table was built with the compounds as rows and two types of column values: 5-HT_{1A} and α_1 pK_i values (dependent variables) and the steric and electrostatic field potential values (independent variables). The introduction of log *P* values did not improve the CoMFA models.

Partial least squares (PLS) methodology[19,20] was used to develop the relationship between the independent variables and the pK_i values. Five orthogonal latent variables were first extracted by standard PLS algorithm and subsequently subjected to a cross-validation in order to correlate them with the dependent variable. If the analysis indicated that more latent variables were required for an optimum description of the variance in the data set, additional PLS runs were performed considering a higher number of components. The "best" model was the one that showed the sum of the squared differences between predicted and observed values of the dependent property to be a minimum from a leave-one-out cross-validation method. The r^2_{cross} values listed for the different models are the maximal values, which were obtained considering the number of components given in the tables. Following the cross-validated analysis a non-cross-validated analysis was performed using the optimum number of components previously identified. The non-cross-validated analyses were used to make predictions of activities and to analyze the CoMFA results. For both the cross-validated and non-cross-validated analyses, the σ used was 2.0 as we found that $\sigma = 1$ or 0.5 did not significantly change the calculated r^2 or SE.

The steric and electrostatic features of the final CoMFA model were displayed as contour plots of the PLS regression coefficients at each CoMFA region grid point. The steric CoMFA contributions were contoured at the 75% and 25% levels, with the "positive" steric contour (75%) colored green and the "negative" steric contour (25%) colored yellow. The electrostatic contribution contours were displayed in similar fashion with red-colored positive contours (interaction of ligands with the positive probe atom in these regions enhances activity) at the 75% level, and blue-colored negative contours (ligand interaction with the positive probe atom in these regions lowers activity) at the 25% level.

Results and Discussion

5-HT_{1A} CoMFA Model. The CoMFA model derived from the potencies of the whole set of analogs (**1a**−**4l**) to inhibit [^{3}H]-8-OH-DPAT binding at the 5-HT_{1A} sites was obtained using the alignment rule discussed in the Methods section. The optimum number of components was selected by identification of the point at which the r^2_{cross} decreased and/or the SE_{cross} increased significantly with respect to the previous values. On the basis of this criteria, eight components were selected ($r^2_{cross} = 0.840$, $SE_{cross} = 0.365$). Table 2 contains the statistics of the CoMFA model derived for the 5-HT_{1A} receptor. The ratio of electrostatic and steric contributions to the final model is 54.4:45.6, respectively. Observed and calculated pK_i values are listed in Table 1 and plotted in Figure 1.

In order to visualize the information content of the derived 3D-QSAR model, CoMFA contour maps were generated by interpolating the products between the 3D-QSAR coefficients and their associated standard deviations. It is worthwhile to remark that these types of contours can only be found in the corresponding areas of the lattice points characterized by variance of the steric and electrostatic properties of the ligands. Thus, their absence does not necessarily mean that a given

Table 1. 5-HT_{1A} Receptor Binding Data[a] with CoMFA Predictions for Derivatives **1**−**4**

compd	X	*n*	R	K_i (nM) ± SEM[b]	p$K_{i\ obsd}$ (nM)	p$K_{i\ calcd}$ (nM)	resid
1a	$-(CH_2)_3-$	1	H	85.3 ± 3.1	−1.93	−1.92	−0.01
1b	$-(CH_2)_3-$	1	*o*-OCH_3	34.9 ± 0.7	−1.54	−1.59	0.05
1c	$-(CH_2)_3-$	1	*m*-Cl	58.4 ± 1.1	−1.77	−1.86	0.09
1d	$-(CH_2)_3-$	1	*m*-CF_3	120 ± 10	−2.08	−2.04	−0.04
1e	$-(CH_2)_3-$	1	*p*-F	500 ± 60	−2.70	−2.91	0.21
1f	$-(CH_2)_3-$	1	*p*-NO_2	6095	−3.79	−3.72	−0.07
1g	$-(CH_2)_4-$	1	H	101 ± 8	−2.01	−2.13	0.12
1h	$-(CH_2)_4-$	1	*o*-OCH_3	31.1 ± 1.7	−1.49	−1.36	−0.13
1i	$-(CH_2)_4-$	1	*m*-Cl	57.7 ± 5.7	−1.76	−1.61	−0.15
1j	$-(CH_2)_4-$	1	*m*-CF_3	78.6 ± 7.5	−1.90	−2.02	0.12
1k	$-(CH_2)_4-$	1	*p*-F	444 ± 52	−2.65	−2.71	0.06
1l	$-(CH_2)_4-$	1	*p*-NO_2	5970	−3.78	−3.87	0.09
2a	$-(CH_2)_3-$	2	H	7550	−3.88	−3.94	0.06
2b	$-(CH_2)_3-$	2	*o*-OCH_3	234 ± 20	−2.37	−2.33	−0.04
2c	$-(CH_2)_3-$	2	*m*-Cl	418 ± 60	−2.62	−2.87	0.25
2d	$-(CH_2)_3-$	2	*m*-CF_3	123 ± 11	−2.09	−2.54	0.45
2e	$-(CH_2)_3-$	2	*p*-F	23932	−4.38	−4.16	−0.22
2f	$-(CH_2)_3-$	2	*p*-NO_2	501187	−5.70	−5.36	−0.34
2g	$-(CH_2)_4-$	2	H	1349	−3.13	−3.17	0.04
2h	$-(CH_2)_4-$	2	*o*-OCH_3	45.5 ± 4.6	−1.66	−1.73	0.07
2i	$-(CH_2)_4-$	2	*m*-Cl	128 ± 10	−2.11	−2.05	−0.06
2j	$-(CH_2)_4-$	2	*m*-CF_3	65.8 ± 3.1	−1.82	−1.70	−0.12
2k	$-(CH_2)_4-$	2	*p*-F	19274	−4.28	−4.14	−0.14
2l	$-(CH_2)_4-$	2	*p*-NO_2	93590	−4.96	−4.89	−0.07
3a	$-(CH_2)_3-$	3	H	19.2 ±1.5	−1.28	−1.31	0.03
3b	$-(CH_2)_3-$	3	*o*-OCH_3	4.4 ± 0.6	−0.64	−0.68	0.04
3c	$-(CH_2)_3-$	3	*m*-Cl	55.9 ±9.1	−1.75	−1.72	−0.03
3d	$-(CH_2)_3-$	3	*m*-CF_3	3.8 ± 0.5	−0.58	−0.67	0.09
3e	$-(CH_2)_3-$	3	*p*-F	1183	−3.07	−2.99	−0.08
3f	$-(CH_2)_3-$	3	*p*-NO_2	168260	−5.23	−5.29	0.06
3g	$-(CH_2)_4-$	3	H	154 ± 10	−2.19	−2.35	0.16
3h	$-(CH_2)_4-$	3	*o*-OCH_3	4.1 ± 0.6	−0.60	−0.51	−0.09
3i	$-(CH_2)_4-$	3	*m*-Cl	53.6 ± 1.5	−1.73	−1.37	−0.36
3j	$-(CH_2)_4-$	3	*m*-CF_3	5.7 ± 0.7	−0.76	−0.75	−0.01
3k	$-(CH_2)_4-$	3	*p*-F	598 ± 70	−2.78	−2.94	0.16
3l	$-(CH_2)_4-$	3	*p*-NO_2	30618	−4.49	−4.47	−0.02
4a	$-(CH_2)_3-$	4	H	24.8 ± 1.4	−1.39	−1.38	−0.01
4b	$-(CH_2)_3-$	4	*o*-OCH_3	5.5 ± 0.7	−0.74	−0.82	0.08
4c	$-(CH_2)_3-$	4	*m*-Cl	11.3 ± 1.0	−1.05	−0.95	−0.10
4d	$-(CH_2)_3-$	4	*m*-CF_3	2.4 ± 0.6	−0.38	−0.28	−0.10
4e	$-(CH_2)_3-$	4	*p*-F	89.9 ± 5.2	−1.95	−1.85	−0.10
4f	$-(CH_2)_3-$	4	*p*-NO_2	23932	−4.38	−4.04	−0.34
4g	$-(CH_2)_4-$	4	H	78.5 ± 6.8	−1.89	−1.44	−0.45
4h	$-(CH_2)_4-$	4	*o*-OCH_3	8.8 ± 0.9	−0.95	−0.96	0.01
4i	$-(CH_2)_4-$	4	*m*-Cl	7.2 ± 0.6	−0.85	−0.95	0.10
4j	$-(CH_2)_4-$	4	*m*-CF_3	9.9 ± 0.9	−0.99	−0.69	−0.30
4k	$-(CH_2)_4-$	4	*p*-F	57.9 ± 3.2	−1.76	−2.17	0.41
4l	$-(CH_2)_4-$	4	*p*-NO_2	2582	−3.41	−3.81	0.40

[a] K_i ± SEM values are derived from two to four experiments performed in triplicate. [b] SEM is indicated when K_i values are obtained from complete DRCs.

Table 2. CoMFA-PLS Analysis Statistics for pK_i Data at 5-HT_{1A} Sites

SE_{cross}	0.365	no. of compounds	48
r^2_{cross}	0.840	no. of components	8
SE	0.206	steric fraction	0.456
r^2	0.981	electrostatic fraction	0.544
F	245.613		

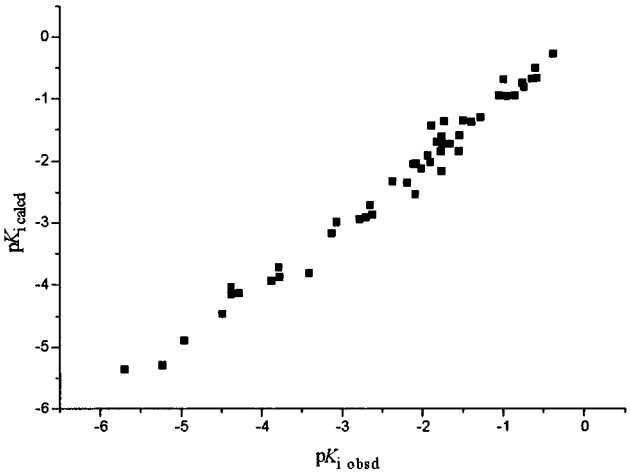

Figure 1. Calculated *vs* observed pK_i values at 5-HT_{1A} receptor sites (n = 48, r = 0.990, s = 0.190, p < 0.001).

pharmacophoric element is actually unimportant, but only that all the examined compounds exert in that area more or less the same steric or electronic influence.

Figures 2−4 show the CoMFA steric and electrostatic contour map using compounds **4b** (X = $-(CH_2)_3-$, n = 4, R = *o*-OCH_3), **4j** (X = $-(CH_2)_4-$, n = 4, R = *m*-CF_3), and **2f** (X = $-(CH_2)_3-$, n = 2, R = *p*-NO_2) as reference structures. The green and yellow polyhedra describe regions of space whose occupancy by the ligands respectively increases or decreases affinity for the 5-HT_{1A} receptor. The green contours around the *ortho* and *meta* positions of the phenyl ring indicate that bulky substituents are tolerated in these positions. However the *para* position is surrounded by a yellow region. This "unfavorable" contour is occupied by the *p*-NO_2 group

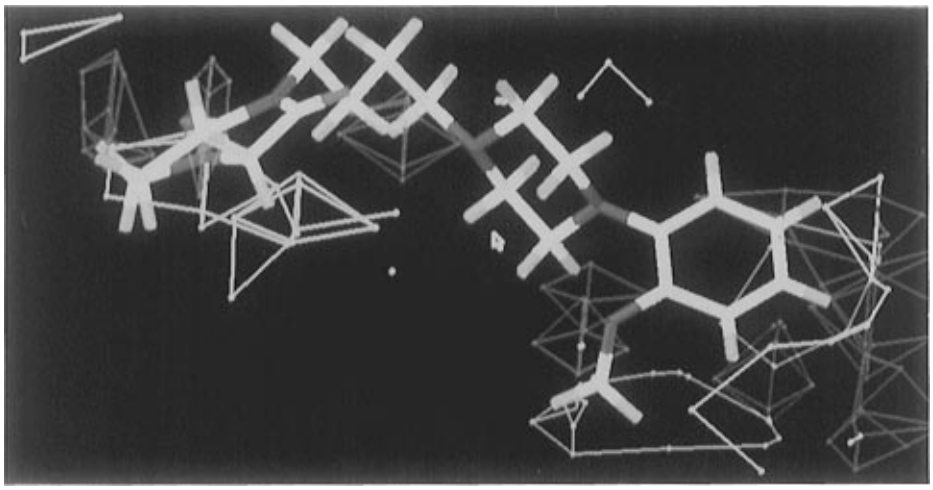

Figure 2. Substitution at the *ortho* position by bulky substituents with negative potential is favorable for 5-HT_{1A} affinity. Molecule displayed is **4b** (X = $-(CH_2)_3-$, n = 4, R = *o*-OCH_3).

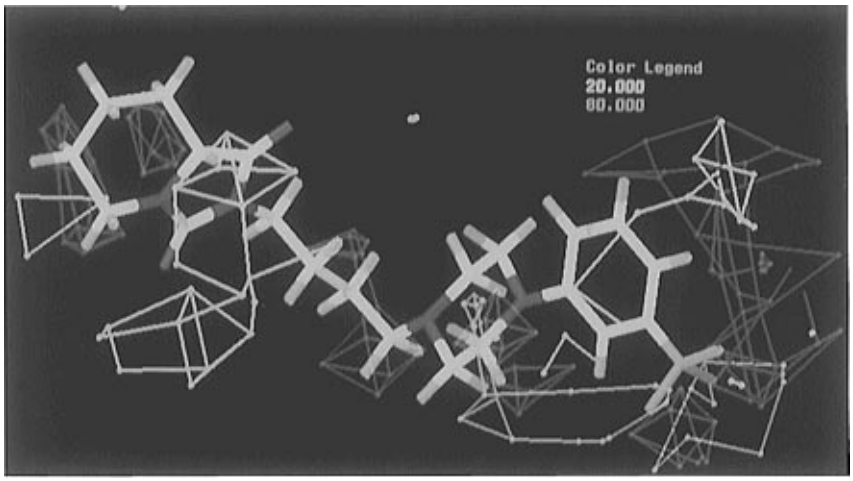

Figure 3. Substitution at the *meta* position by bulky substituents with negative potential is favorable for 5-HT_{1A} affinity. Molecule displayed is **4j** (X = $-(CH_2)_4-$, n = 4, R = *m*-CF_3).

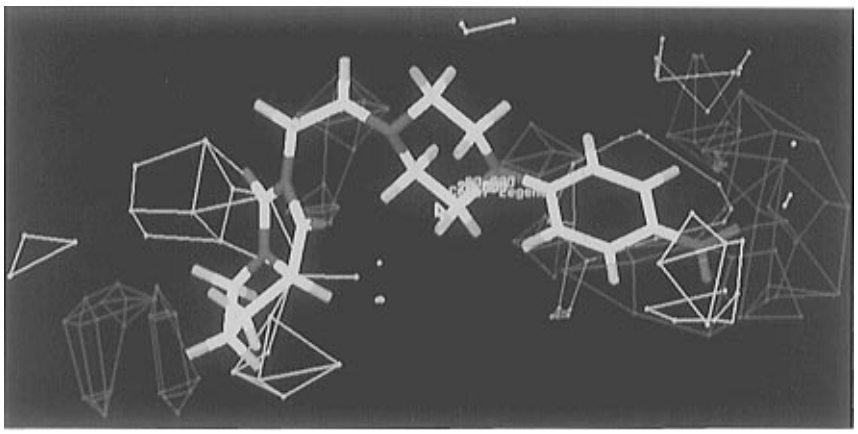

Figure 4. The yellow and blue zones close to the *para* position indicate that bulky and electron-withdrawing substituents can make a negative contribution. Yellow contours close to the hydantoin moiety represent an unfavorable bulk interaction for compounds with n = 1 and especially n = 2. Molecule displayed is **2f** (X = $-(CH_2)_3-$, n = 2, R = *p*-NO_2).

and is related to the presence of a steric restriction in the receptor cavity delimiting the volume accessible to the ligands. If this hypothesis is correct, bulky substituents at this position, no matter their electrostatic properties, would cause a strong decrease of potency. In order to prove this assumption, a new ligand bearing an electron-donating amino group at this position, **4m** (X = $-(CH_2)_3-$, n = 4, R = *p*-NH_2), was synthesized, leading, as expected, to an inactive compound (K_i > 10 000 nM). Finally, another important yellow region is located around the hydantoin moiety of the short-chain molecules. This appears to suggest that an unfavorable bulky interaction would be involved in the decrease of affinity observed for derivatives with n = 1 and especially with n = 2.

The electrostatic contour maps are represented by red and blue polyhedra describing regions where a high electron density within the ligand structure increases

Table 3. Statistical Parameters Derived for the 5-HT_{1A} Receptor CoMFA-PLS Analysis Model Used for Predictions

SE_{cross}	0.360	no. of compounds	42
r^2_{cross}	0.825	no. of components	7
SE	0.202	steric fraction	0.399
r^2	0.978	electrostatic fraction	0.601
F	229.726		

Table 4. Observed *vs* Predicted 5-HT_{1A} Receptor Binding Values (pK_i, nM)

compd	X	n	R	$pK_{i\ obsd}$	$pK_{i\ pred}$	resid
1d	$-(CH_2)_3-$	1	*m*-CF_3	−2.08	−1.89	−0.19
2f	$-(CH_2)_3-$	2	*p*-NO_2	−5.70	−5.00	−0.70
2k	$-(CH_2)_4-$	2	*p*-F	−4.28	−3.88	−0.40
3c	$-(CH_2)_3-$	3	*m*-Cl	−1.75	−1.40	−0.35
4b	$-(CH_2)_3-$	4	*o*-OCH_3	−0.74	−0.89	0.15
4g	$-(CH_2)_4-$	4	H	−1.89	−1.34	−0.55

or decreases, respectively, the affinity. The red contours surrounding the *ortho* and *meta* positions show that negative potentials in such positions increase the 5-HT_{1A} affinity. The blue polyhedron in the *para* position indicates that electron-withdrawing substituents exert a negative effect on the affinity. This seems to suggest that positive potentials in that region of the phenyl ring enhance the potency. However the strong steric hindrance at this position restricts completely the substitution.

In order to evaluate the predictive capacity of the CoMFA model, six molecules (**1d**, **2f**, **2k**, **3c**, **4b**, and **4g**) were removed from the original data set ($n = 48$) used in the previous CoMFA. The molecules were chosen on the basis of their affinity (one with high, two with low, and three with moderate affinity). CoMFA was redone for the remaining 42 compounds. The CoMFA results for the 42 compounds are presented in Table 3. This CoMFA was applied to the six omitted compounds. A comparison of the observed and predicted values for the six compounds tested shows an acceptable agreement overall (Table 4).

α_1 CoMFA Model. A set of 42 molecules was used in the CoMFA study (Table 5). The molecules **1h**, **2a**, **2e**, **2g**, **2k**, and **4l** were not included in the analysis in order to keep a balance between active and inactive molecules. These compounds were used later as a test set to investigate the predictive power of the derived model. The stepwise F-test performed on the PRESS values justified seven components with $SE_{cross} = 0.287$ and $r^2_{cross} = 0.809$. As expected, the corresponding non-

Table 5. α_1 Receptor Binding Data[a] with CoMFA Predictions for Derivatives **1**−**4**

compd	X	n	R	K_i (nM) ± SEM[b]	$pK_{i\ obsd}$ (nM)	$pK_{i\ calcd}$ (nM)	resid
1a	$-(CH_2)_3-$	1	H	2588	−3.41	−3.19	−0.22
1b	$-(CH_2)_3-$	1	*o*-OCH_3	500 ± 65	−2.70	−2.76	0.06
1c	$-(CH_2)_3-$	1	*m*-Cl	292 ± 15	−2.47	−2.57	0.10
1d	$-(CH_2)_3-$	1	*m*-CF_3	3296	−3.52	−3.15	−0.37
1e	$-(CH_2)_3-$	1	*p*-F	1193	−3.08	−3.38	0.30
1f	$-(CH_2)_3-$	1	*p*-NO_2	260000	−5.41	−5.44	0.03
1g	$-(CH_2)_4-$	1	H	2075	−3.32	−3.46	0.14
1i	$-(CH_2)_4-$	1	*m*-Cl	135 ± 5	−2.13	−2.22	0.09
1j	$-(CH_2)_4-$	1	*m*-CF_3	3296	−3.52	−3.47	−0.05
1k	$-(CH_2)_4-$	1	*p*-F	869 ± 75	−2.94	−2.82	−0.12
1l	$-(CH_2)_4-$	1	*p*-NO_2	260000	−5.41	−5.30	−0.11
2b	$-(CH_2)_3-$	2	*o*-OCH_3	190 ± 38	−2.28	−2.40	0.12
2c	$-(CH_2)_3-$	2	*m*-Cl	500 ± 65	−2.70	−2.81	0.11
2d	$-(CH_2)_3-$	2	*m*-CF_3	3935	−3.60	−3.65	0.05
2f	$-(CH_2)_3-$	2	*p*-NO_2	260000	−5.40	−5.24	−0.16
2h	$-(CH_2)_4-$	2	*o*-OCH_3	131 ± 28	−2.12	−2.31	0.19
2i	$-(CH_2)_4-$	2	*m*-Cl	375 ± 16	−2.57	−2.67	0.10
2j	$-(CH_2)_4-$	2	*m*-CF_3	4325	−3.64	−3.52	−0.12
2l	$-(CH_2)_4-$	2	*p*-NO_2	199000	−5.30	−5.21	−0.09
3a	$-(CH_2)_3-$	3	H	15.4 ± 3.9	−1.19	−1.15	−0.04
3b	$-(CH_2)_3-$	3	*o*-OCH_3	3.1 ± 0.5	−0.49	−0.52	0.03
3c	$-(CH_2)_3-$	3	*m*-Cl	21.6 ± 1.1	−1.33	−1.44	0.11
3d	$-(CH_2)_3-$	3	*m*-CF_3	109 ± 9	−2.04	−1.95	−0.09
3e	$-(CH_2)_3-$	3	*p*-F	25.2 ± 1.1	−1.40	−1.31	−0.09
3f	$-(CH_2)_3-$	3	*p*-NO_2	7533	−3.88	−3.70	−0.18
3g	$-(CH_2)_4-$	3	H	11.4 ± 0.9	−1.06	−0.81	−0.25
3h	$-(CH_2)_4-$	3	*o*-OCH_3	9.9 ± 1.0	−1.00	−0.90	−0.10
3i	$-(CH_2)_4-$	3	*m*-Cl	17.9 ± 1.1	−1.24	−1.32	0.08
3j	$-(CH_2)_4-$	3	*m*-CF_3	90.4 ± 5.1	−1.96	−2.07	0.11
3k	$-(CH_2)_4-$	3	*p*-F	25.8 ± 1.1	−1.41	−1.54	0.13
3l	$-(CH_2)_4-$	3	*p*-NO_2	6652	−3.82	−4.04	0.22
4a	$-(CH_2)_3-$	4	H	26.4 ± 1.9	−1.42	−1.29	−0.13
4b	$-(CH_2)_3-$	4	*o*-OCH_3	8.3 ± 0.3	−0.92	−0.90	−0.02
4c	$-(CH_2)_3-$	4	*m*-Cl	9.6 ± 0.9	−0.98	−0.97	−0.01
4d	$-(CH_2)_3-$	4	*m*-CF_3	64.9 ± 2.6	−1.81	−1.72	−0.09
4e	$-(CH_2)_3-$	4	*p*-F	47.2 ± 1.8	−1.67	−1.53	−0.14
4f	$-(CH_2)_3-$	4	*p*-NO_2	247 ± 63	−2.39	−2.63	0.24
4g	$-(CH_2)_4-$	4	H	18.6 ± 3.1	−1.27	−1.10	−0.17
4h	$-(CH_2)_4-$	4	*o*-OCH_3	8.6 ± 1.0	−0.94	−0.98	0.04
4i	$-(CH_2)_4-$	4	*m*-Cl	12.1 ± 1.2	−1.08	−0.81	−0.27
4j	$-(CH_2)_4-$	4	*m*-CF_3	72.4 ± 8.0	−1.86	−2.05	0.19
4k	$-(CH_2)_4-$	4	*p*-F	10.4 ± 0.6	−1.02	−1.41	0.39

[a] K_i ± SEM values are derived from two to four experiments performed in triplicate. [b] SEM is indicated when K_i values are obtained from complete DRCs.

Table 6. CoMFA-PLS Analysis Statistics for pK_i Data at α_1 Sites

SE_{cross}	0.287	no. of compounds	42
r^2_{cross}	0.809	no. of components	7
SE	0.179	steric fraction	0.390
r^2	0.985	electrostatic fraction	0.610
F	329.391		

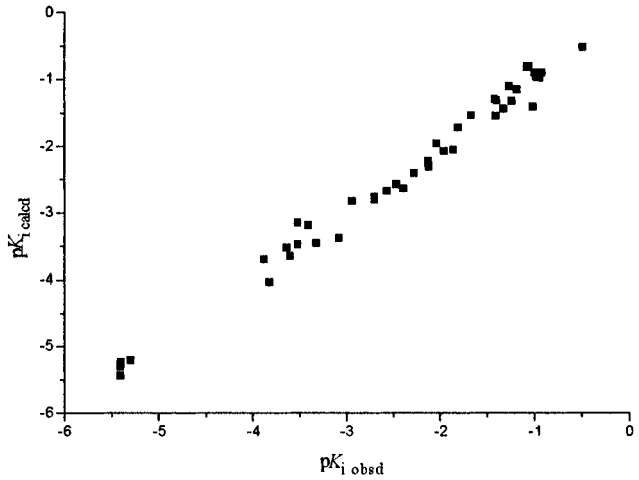

Figure 5. Calculated *vs* observed pK_i at the α_1 receptor site ($n = 42$, $r = 0.992$, $s = 0.164$, $p < 0.001$).

cross-validated analysis yields a better data fitting (SE = 0.179 and $r^2 = 0.985$) (Table 6). The ratio of electrostatic and steric contributions to the final model is 61:39, respectively. Observed and calculated pK_i values are reported in Table 5 and plotted in Figure 5.

Figures 6−8 show the contributions of the steric and electrostatic fields to the CoMFA model. The green polyhedra around the *ortho* and *meta* positions suggest that the occupation of those regions increases affinity. However the *meta* position presents an optimum volume of substituent between 11 and 25 Å^3 (the V_W of chloro and CF_3 group, respectively). Thus, while a chloro substituent exerts a modest positive effect, the introduction of a CF_3 group decreases slightly the affinity. Figure 7 shows that the *m*-CF_3 group reaches an adjacent yellow zone, which extends around the whole *para* position. The CoMFA model describes the loss of potency associated with the *p*-nitro substitution as a strong unfavorable bulk interaction.

The red contours surrounding the *ortho* and *meta* positions show that the presence of negative potentials in those regions leads to an increase of affinity. The interpretation of the inner red and the outer blue polyhedra located near the *para* position is more complex. The presence of a fluoro substituent at the *para* position of the phenylpiperazine system leads to a moderate increase of affinity. This effect is described by the red contours located in the corresponding areas of the *p*-fluoro derivatives. The blue polyhedra take into account the about 100-fold drop of affinity observed when a nitro group is introduced at this position. However, such a contour should not be overemphasized since the loss of activity of the *p*-NO_2 derivatives can

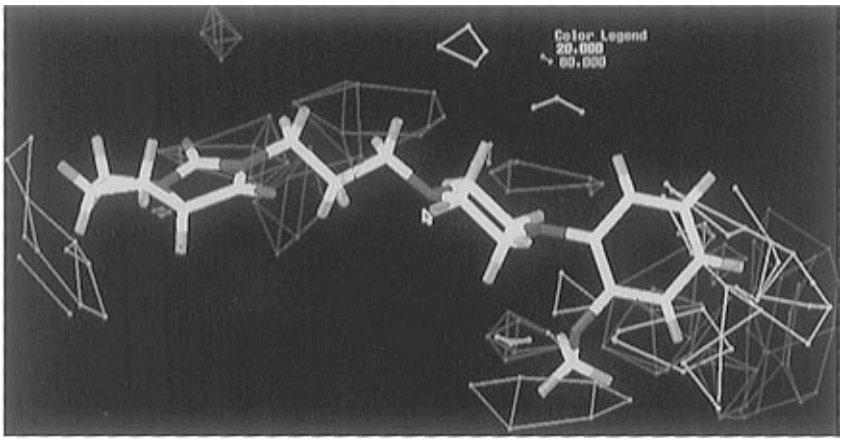

Figure 6. Substitution at the *ortho* position by bulky substituents with negative potential is favorable for affinity. Molecule displayed is **3b** (X = $-(CH_2)_3-$, $n = 3$, R = *o*-OCH_3).

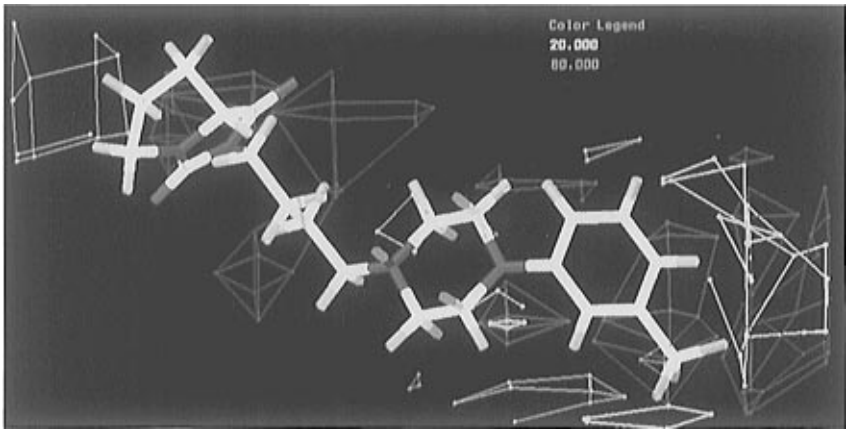

Figure 7. The yellow region close to the *meta* position indicates that too bulky groups decrease affinity. Molecule displayed is **4d** (X = $-(CH_2)_3-$, $n = 4$, R = *m*-CF_3).

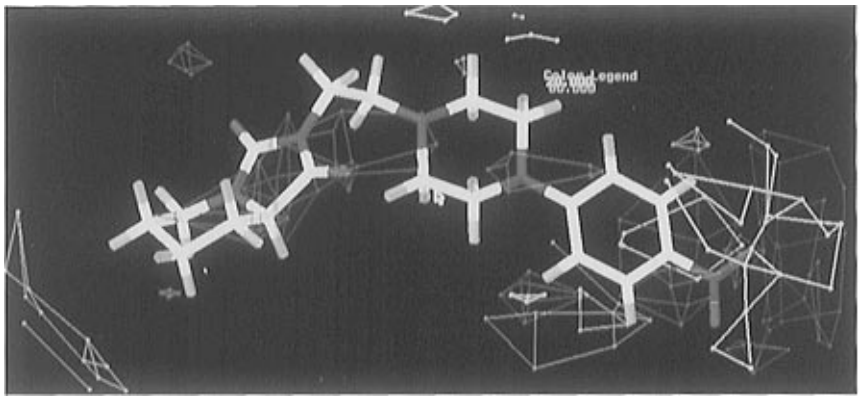

Figure 8. A bulky substituent with negative potential at the *para* position can make a negative contribution. Molecule displayed is **2l** (X = $-(CH_2)_4-$, n = 2, R = p-NO_2).

Table 7. Observed *vs* Predicted α_1 Receptor Binding Values (pK_i, nM)

compd	X	n	R	$pK_{i\ obsd}$	$pK_{i\ pred}$
1h	$-(CH_2)_4-$	1	o-OCH_3	<−3	−2.94
2a	$-(CH_2)_3-$	2	H	<−3	−3.11
2e	$-(CH_2)_3-$	2	p-F	<−3	−3.35
2g	$-(CH_2)_4-$	2	H	<−3	−2.90
2k	$-(CH_2)_4-$	2	p-F	<−3	−3.46
4l	$-(CH_2)_4-$	4	p-NO_2	<−3	−2.92

be due to an undesired bulk interaction. This is supported by the loss of affinity exhibited by the ligand **4m** (R = p-NH_2) (K_i > 1000 nM). This proves that the potency of the *para*-substituted derivatives is modulated mainly by steric factors and not by electrostatic ones. Finally, the blue contour in the proximity of the hydantoin moiety describes the detrimental effect on affinity caused by the shortening of the chain.

As already mentioned, compounds **1h**, **2a**, **2e**, **2g**, **2k**, and **4l** allow us to evaluate the efficiency of the derived CoMFA model in estimating binding affinity values for structures outside the training set. Table 7 lists the observed pK_i values of the compounds belonging to the test set together with the corresponding pK_i values predicted by the CoMFA model.

Comparison of CoMFA Models. Comparison of the CoMFA contour maps generated for both analyses gives an additional understanding for 5-HT_{1A}/α_1 selectivity, leading to four important conclusions. (a) Substitution at the *ortho* position by a group with negative potential is favorable to affinity for both receptors.

(b) The *meta* position seems to be implicated in 5-HT_{1A}/α_1 selectivity. While the 5-HT_{1A} receptor is able to accommodate bulky substituents in the region of its active site, the steric requirements of the α_1 receptor at this position are more restricted. In addition the α_1 receptor exhibits an optimum volume of substituent (11−25 Å^3).

(c) For both receptors the *para* position represents a region where the volume accessible by the ligands is limited. Only very small substituents, like fluoro, can be accommodated in the receptor pocket.

(d) Finally, both structural features, the hydantoin moiety and the side chain length, seem to modulate not only the affinity, but also the 5-HT_{1A}/α_1 selectivity. Thus the compounds with n = 1 present a moderate potency at the 5-HT_{1A} receptor and are much less active at the α_1 receptor.

These results suggest that a good way to improve 5-HT_{1A}/α_1 selectivity would be the synthesis of long-chain derivatives bearing bulky substituents with negative potential at the *meta* position. Thus, the new ligand **4n** (X = $-(CH_2)_3-$, n = 4, R = m-NHCOPr^i) was designed and synthesized. This analog bound at 5-HT_{1A} sites (K_i = 102 ± 8 nM) and exhibited high selectivity over the α_1 receptor (K_i > 10000 nM). Although the potency of **4n** at the 5-HT_{1A} receptor is moderate, the high 5-HT_{1A}/α_1 selectivity supports our CoMFA models and affords insights for the design of new selective compounds. In order to increase the affinity for the 5-HT_{1A} receptor, further synthesis and biological evaluation of new derivatives structurally related to **4n** are in progress, and the results will be reported in due course.

In conclusion, the CoMFA method has been successfully applied to a set of recently described hydantoin−phenylpiperazines with affinity for 5-HT_{1A} and α_1 receptors. The resulting 3D-QSAR models provide significant correlation of steric and electrostatic fields with the biological affinities. The CoMFA coefficient contour plots provide a self-consistent picture of the main chemical features responsible for the pK_i variations and also result in predictions which agree with experimental values. By comparison of the CoMFA models, suggestions can be made about the improvement of 5-HT_{1A}/α_1 selectivity. This information seems to be very useful for the design of new agents possessing high selectivity for 5-HT_{1A} *vs* α_1 receptors.

Experimental Section

Chemistry. Melting points (uncorrected) were determined on a Gallenkamp electrothermal apparatus. Infrared (IR) spectra were obtained on a Perkin-Elmer 781 infrared spectrophotometer. ^{1}H- and ^{13}C-NMR spectra were recorded on a Varian VXR-300S or Bruker 250-AM instrument. Chemical shifts (δ) are expressed in parts per million relative to internal tetramethylsilane; coupling constants (J) are in hertz. Elemental analyses (C, H, N) were determined within 0.4% of the theoretical values. Thin-layer chromatography (TLC) was run on Merck silica gel 60 F-254 plates. For flash chromatography, Merck silica gel type 60 (size 230−400 mesh) was used. Unless stated otherwise, starting materials were used as high-grade commercial products.

The following compounds were synthesized by published procedures: 1,3-dioxoperhydropyrrolo[1,2-*c*]imidazole,[21] 1-(*m*-nitrophenyl)piperazine,[22] 2-(4-bromobutyl)-1,3-dioxoperhydropyrrolo[1,2-*c*]imidazole,[1] and 2-[4-[4-(*p*-nitrophenyl)piperazin-1-yl]butyl]-1,3-dioxoperhydropyrrolo[1,2-*c*]imidazole (**4f**).[1]

2-[4-[4-(*m*-Nitrophenyl)piperazin-1-yl]butyl]-1,3-dioxoperhydropyrrolo[1,2-*c*]imidazole (4o). To a suspension of 2-(4-bromobutyl)-1,3-dioxoperhydropyrrolo[1,2-*c*]imidazole (2.6 g, 9.5 mmol) and 1-(*m*-nitrophenyl)piperazine (3.0 g, 14.6

mmol) in acetonitrile (19 mL) was added 2.0 mL of triethylamine (1.5 g, 14.6 mmol). The mixture was refluxed for 20−24 h. Then, the solvent was evaporated under reduced pressure, and the residue was resuspended in water and extracted with dichloromethane (3 × 100 mL). The combined organic layers were washed with water and dried over $MgSO_4$. After evaporation of the solvent the crude oil was purified by column chromatography (ethyl acetate/ethanol, 9:1) to give 2.21 g (58%) of **4o**, which was converted to its hydrochloride salt: mp 197−198 °C (methanol/ethyl ether); IR ($CHCl_3$, cm^{-1}) 1770 (CON), 1710 (NCON), 1620, 1580, 1500, 1450 (Ar), 1530 (NO_2); ^{1}H-NMR ($CDCl_3$, as free base) δ 1.43−1.66 (m, 5H, $-(CH_2)_2-$, H_7), 1.94−2.06 (m, 2H, $2H_6$), 2.13−2.22 (m, 1H, H_7), 2.35 (t, J = 7.4 Hz, 2H, CH_2-Npip), 2.52 (t, J = 5.1 Hz, 4H, $2CH_2$-pip), 3.15−3.23 (m, 5H, $2CH_2$-pip, H_5), 3.43 (t, J = 7.0 Hz, 2H, NCH_2), 3.61 (dt, J = 11.7, 7.7 Hz, 1H, H_5), 4.02 (dd, J = 9.0, 7.7 Hz, 1H, H_{7a}), 7.10 (dd, J = 8.3, 2.2 Hz, 1H, H_6-phenyl), 7.29 (t, J = 8.2 Hz, 1H, H_5-phenyl), 7.56 (dd, J = 8.0, 1.2 Hz, 1H, H_4-phenyl), 7.62 (t, J = 2.1 Hz, 1H, H_2-phenyl); ^{13}C-NMR ($CDCl_3$, as free base) δ 24.0, 26.0 ($-(CH_2)_2-$), 27.1 (C_6), 27.6 (C_7), 38.8 (NCH_2), 45.6 (C_5), 48.3 ($2CH_2$-pip), 52.9 ($2CH_2$-pip), 57.9 (CH_2-Npip), 63.4 (C_{7a}), 109.6 (C_2-phenyl), 113.6 (C_4-phenyl), 121.1 (C_6-phenyl), 129.7 (C_5-phenyl), 149.3 (C_1-phenyl), 151.9 (C_3-phenyl), 160.9 (C_3), 174.1 (C_1). Anal. ($C_{20}H_{27}N_5O_4$·HCl) C, H, N.

General Procedure. Preparation of Compounds 4m and 4p. To a solution of **4f,o** (5 mmol) in methanol (18 mL) was added 0.1 g of 10% Pd(C). The mixture was hydrogenated (35 psi) at room temperature for 2 h. The reaction mixture was filtered over Celite and evaporated to dryness to afford the pure amines. The free base was converted to its hydrochloride salt.

2-[4-[4-(*p*-Aminophenyl)piperazin-1-yl]butyl]-1,3-dioxoperhydropyrrolo[1,2-*c*]imidazole (4m): yield 1.62 g (87%); mp 281−284 °C (methanol/ethyl ether); IR (KBr, cm^{-1}) 3420, 3350, 3220 (NH_2), 1770 (CON), 1700 (NCON), 1520, 1450 (Ar); ^{1}H-NMR ($CDCl_3$, as free base) δ 1.40−1.66 (m, 5H, $-(CH_2)_2-$, H_7), 1.91−2.04 (m, 2H, $2H_6$), 2.12−2.22 (m, 1H, H_7), 2.33 (t, J = 7.2 Hz, 2H, CH_2-Npip), 2.51 (t, J = 4.8 Hz, 4H, $2CH_2$-pip), 2.97 (t, J = 4.8 Hz, 4H, $2CH_2$-pip), 3.12−3.20 (m, 1H, H_5), 3.32 (sa, 2H, NH_2), 3.42 (t, J = 7.2 Hz, 2H, NCH_2), 3.60 (dt, J = 11.4, 7.5 Hz, 1H, H_5), 3.99 (dd, J = 8.1, 7.5 Hz, 1H, H_{7a}), 6.57 (d, J = 8.7 Hz, 2H, H_3- and H_5-phenyl), 6.73 (d, J = 8.7 Hz, 2H, H_2- and H_6-phenyl); ^{13}C-NMR ($CDCl_3$, as free base) δ 23.9, 25.9 ($-(CH_2)_2-$), 26.9 (C_6), 27.4 (C_7), 38.7 (NCH_2), 45.4 (C_5), 50.7 ($2CH_2$-pip), 53.2 ($2CH_2$-pip), 57.9 (CH_2-Npip), 63.2 (C_{7a}), 116.0 (C_2- and C_6-phenyl), 118.4 (C_3- and C_5-phenyl), 140.0 (C_4-phenyl), 144.4 (C_1-phenyl), 160.7 (C_3), 173.8 (C_1). Anal. ($C_{20}H_{29}N_5O_2$·2HCl·$^1/_2H_2O$) C, H, N.

2-[4-[4-(*m*-Aminophenyl)piperazin-1-yl]butyl]-1,3-dioxoperhydropyrrolo[1,2-*c*]imidazole (4p): yield 1.73 g (93%); mp 92−94 °C (methanol/ethyl ether); IR ($CHCl_3$, cm^{-1}) 3120−3600 (NH_2), 1770 (CON), 1700 (NCON), 1600, 1500, 1450 (Ar); ^{1}H-NMR ($CDCl_3$, as free base) δ 1.45−1.65 (m, 5H, $-(CH_2)_2-$, H_7), 1.96−2.04 (m, 2H, $2H_6$), 2.13−2.23 (m, 1H, H_7), 2.35 (t, J = 7.5 Hz, 2H, CH_2-Npip), 2.52 (t, J = 5.1 Hz, 4H, $2CH_2$-pip), 3.10 (t, J = 4.8 Hz, 4H, $2CH_2$-pip), 3.15−3.21 (m, 1H, H_5), 3.42 (t, J = 7.2 Hz, 2H, NCH_2), 3.59 (dt, J = 11.1, 7.5 Hz, 1H, H_5), 4.00 (dd, J = 9.0, 7.5 Hz, 1H, H_{7a}), 6.14 (dd, J = 8.1, 1.5 Hz, 1H, H_4-phenyl), 6.17 (t, J = 1.8 Hz, 1H, H_2-phenyl), 6.27 (dd, J = 7.8, 1.8 Hz, 1H, H_6-phenyl), 6.96 (t, J = 7.8 Hz, 1H, H_5-phenyl); ^{13}C-NMR ($CDCl_3$, as free base) δ 23.7, 25.9 ($-(CH_2)_2-$), 26.9 (C_6), 27.4 (C_7), 38.6 (NCH_2), 45.4 (C_5), 48.8 ($2CH_2$-pip), 53.0 ($2CH_2$-pip), 57.8 (CH_2-Npip), 63.2 (C_{7a}), 102.7 (C_2-phenyl), 106.7, 106.9 (C_4- and C_6-phenyl), 129.7 (C_5-phenyl), 147.2 (C_3-phenyl), 152.3 (C_1-phenyl), 160.7 (C_3), 173.9 (C_1). Anal. ($C_{20}H_{29}N_5O_2$·3HCl) C, H, N.

2-[4-[4-[*m*-(2-Methylpropanamido)phenyl]piperazin-1-yl]butyl]-1,3-dioxoperhydropyrrolo[1,2-*c*]imidazole (4n). To a solution of **4p** (1.7 g, 4.6 mmol) in pyridine (52 mL) at 0 °C was added dropwise 0.5 mL of isobutyryl chloride (0.49 g, 4.6 mmol). After being stirred at room temperature for 1.5 h, the mixture was washed with a saturated aqueous solution of $CuSO_4$, water, and a saturated aqueous solution of NaCl (brine). The organic layer was dried ($NaSO_4$) and the solvent evaporated under reduced pressure to afford 1.25 g (62%) of **4n**, which was converted to its hydrochloride salt: mp 189−192 °C (methanol/ethyl ether); IR ($CHCl_3$, cm^{-1}) 3060−3300 (NH), 1770 (CON), 1700 (NCON), 1650 (CONH), 1610, 1500, 1450 (Ar); ^{1}H-NMR ($CDCl_3$, as free base) δ 1.16 (d, J = 6.6 Hz, 6H, $2CH_3$), 1.42−1.67 (m, 5H, $-(CH_2)_2-$, H_7), 1.97−2.04 (m, 2H, $2H_6$), 2.18−2.22 (m, 1H, H_7), 2.32 (t, J = 7.5 Hz, 2H, CH_2-Npip), 2.41−2.49 (m, 5H, $2CH_2$-pip, CH), 3.10−3.21 (m, 5H, $2CH_2$-pip, H_5), 3.42 (t, J = 7.5 Hz, 2H, NCH_2), 3.60 (dt, J = 11.1, 7.5 Hz, 1H, H_5), 4.00 (dd, J = 7.5, 7.2 Hz, 1H, H_{7a}), 6.57 (dd, J = 8.4, 2.1 Hz, 1H, H_6-phenyl), 6.76 (d, J = 7.8 Hz, 1H, H_4-phenyl), 7.08 (t, J = 7.8 Hz, 1H, H_5-phenyl), 7.34 (s, 1H, H_2-phenyl), 7.41 (s, 1H, CONH); ^{13}C-NMR ($CDCl_3$, as free base) δ 19.8 ($2CH_3$), 24.0, 26.1 ($-(CH_2)_2-$), 27.1 (C_6), 27.6 (C_7), 36.8 (CH), 38.9 (NCH_2), 45.6 (C_5), 48.9 ($2CH_2$-pip), 53.2 ($2CH_2$-pip), 58.0 (CH_2-Npip), 63.4 (C_{7a}), 107.4 (C_2-phenyl), 110.6, 111.5 (C_4- and C_6-phenyl), 129.4 (C_5-phenyl), 139.2 (C_3-phenyl), 152.0 (C_1-phenyl), 160.9 (C_3), 174.1 (C_1), 175.5 (CONH). Anal. ($C_{24}H_{35}N_5O_3$·2HCl·H_2O) C, H, N.

Radioligand Binding Assays. For all receptor binding assays, male Sprague−Dawley rats (*Rattus norvegicus albinus*), weighing 180−200 g, were killed by decapitation and the brains rapidly removed and dissected.

5-HT_{1A} Receptor. The receptor binding studies were performed by a modification of a previously described procedure.[23] The cerebral cortex was homogenized in 10 volumes of ice-cold Tris-buffer (50 mM Tris-HCl, pH 7.7, at 25 °C) and centrifuged at 28000*g* for 15 min. The membrane pellet was washed twice by resuspension and centrifugation. After the second wash the resuspended pellet was incubated at 37 °C for 10 min. Membranes were then collected by centrifugation, and the final pellet was resuspended in 50 mM Tris-HCl, 5 mM $MgSO_4$, and 0.5 mM EDTA buffer (pH 7.4 at 37 °C). Fractions of the final membrane suspension (about 1 mg of protein) were incubated at 37 °C for 15 min with 0.6 nM [^{3}H]-8-OH-DPAT [8-hydroxy-2-(di-*n*-propylamino)tetralin] (133 Ci/mmol) in the presence or absence of several concentrations of the competing drug, in a final volume of 1.1 mL of assay buffer (50 mM Tris-HCl, 10 nM clonidine, 30 nM prazosin, pH 7.4 at 25 °C). Nonspecific binding was determined with 10 μM 5-HT.

α_1 Adrenoceptor. The radioligand receptor binding studies were performed according to a previously described procedure.[24] The cerebral cortex was homogenized in 20 volumes of ice-cold buffer (50 mM Tris-HCl, 10 mM $MgCl_2$, pH 7.7 at 25 °C) and centrifuged at 30000*g* for 15 min. Pellets were washed twice by resuspension and centrifugation. Final pellets were resuspended in the same buffer. Fractions of the final membrane suspension (about 250 μg of protein) were incubated at 25 °C for 30 min with 0.2 nM [^{3}H]prazosin (23 Ci/mmol) in the presence or absence of several concentrations of the competing drug, in a final volume of 2 mL of buffer. Nonspecific binding was determined with 10 μM phentolamine.

Acknowledgment. This work was supported by DGICYT (PB940289) and the Universidad Complutense (PR218/94-5657). The authors are grateful to MEC for an FPI grant to M. L. Rosado, and to UNED for predoctoral grants to B. Benhamú and E. Fernández.

References

(1) López-Rodríguez, M. L.; Rosado, M. L.; Benhamú, B.; Morcillo, M. J.; Sanz, A. M.; Orensanz, L.; Beneytez, M. E.; Fuentes, J. A.; Manzanares, J. Synthesis and Structure-Activity Relationships of a New Model of Arylpiperazines. 1. 2-[[4-(*o*-Methoxyphenyl)piperazin-1-yl]methyl]-1,3-dioxoperhidroimidazo[1,5-*a*]-pyridine: A Selective 5-HT_{1A} Receptor Agonist. *J. Med. Chem.* **1996**, *39*, 4439−4450.

(2) Portions of this research were presented at the 11th European Symposium on Quantitative Structure-Activity Relationships: Computer-Assisted Lead Finding and Optimization, Lausanne, Switzerland, September 1−6, 1996; abstract p P-29.D.

(3) Fargin, A.; Raymond, J. R.; Lohse, M. J.; Kobilka, B. K.; Caron, M. G.; Lefkowitz, R. J. The Genomic Clone G-21 which Resembles a β-Adrenergic Receptor Sequence Encodes the 5-HT_{1A} Receptor. *Nature* **1988**, *335*, 358−360.

(4) Libert, F.; Parmentier, M.; Lefort, A.; Dinsart, C.; Van Sande, J.; Maenhaut, C.; Simons, M.-J.; Dumont, J. E.; Vassart, G. Selective Amplification and Cloning of Four New Members of the G Protein-Coupled Receptor Family. *Science* **1989**, *244*, 569−572.
(5) Hoflack, J.; Trumpp-Kallmeyer, S.; Hibert, M. F. Molecular Modelling of G Protein-Coupled Receptors. In *3D QSAR in Drug Design. Theory Methods and Applications*; Kubinyi, H., Ed.; ESCOM Science Publishers: Leiden, 1993; pp 355−372.
(6) El-Bermawy, M.; Raghupathi, R.; Ingher, S. P.; Teitler, M.; Maayani, S.; Glennon, R. A. 4-[4-(1-Noradamantanecarboxamido)butyl]-1-(2-methoxyphenyl)piperazine: a High-Affinity 5-HT_{1A}-Selective Agent. *Med. Chem. Res.* **1992**, *2*, 88−95.
(7) Mokrosz, M. J.; Chojnacka-Wójcik, E.; Tatarczyńska, E.; Klodzińska, A.; Filip, M.; Boksa, J.; Charakchieva-Minol, S.; Mokrosz, J. L. 1-(2-Methoxyphenyl)-4-[(4-succinimido)butyl]piperazine (MM-77): A New, Potent, Postsynaptic Antagonist of 5-HT_{1A} Receptors. *Med. Chem. Res.* **1994**, *4*, 161−169.
(8) López-Rodríguez, M. L.; Morcillo, M. J.; Rosado, M. L.; Benhamú, B.; Sanz, A. M. 2-[[4-(*o*-Methoxyphenyl)piperazin-1-yl]methyl]-1,3-dioxoperhidroimidazo[1,5-*a*]pyridine as a New Selective 5-HT_{1A} Receptor Ligand. *Bioorg. Med. Chem. Lett.* **1996**, *6*, 689−694.
(9) Hibert, M. F.; Gittos, M. W.; Middlemiss, D. N.; Mir, A. K.; Fozard, J. R. Graphics Computer-Aided Receptor Mapping as a Predictive Tool for Drug Design: Development of Potent, Selective and Stereospecific Ligands for the 5-HT_{1A} Receptor. *J. Med. Chem.* **1988**, *31*, 1087−1093.
(10) El-Bermawy, M. A.; Lotter, H.; Glennon, R. A. Comparative Molecular Field Analysis of the Binding of Arylpiperazines at 5-HT_{1A} Serotonin Receptors. *Med. Chem. Res.* **1992**, *2*, 290−297.
(11) Mokrosz, J. L.; Duszynska, B. Structure-Activity Relationships Studies of CNS Agents. Part VII. The Effect of the Imidazole Fragment in 2-Substituted 1-[3-(4-Aryl-1-piperazinyl)propyl]-imidazoles on their Interaction Modes with 5-HT_{1A} and 5-HT_2 Receptors. *Pol. J. Pharmacol. Pharm.* **1992**, *44*, 527−538.
(12) Campbell, S. F.; Davey, M. J.; Hardstone, J. D.; Lewis, B. N.; Palmer, M. J. 2,4-Diamino-6,7-dimethoxyquinazolines. 1. 2-[4-(1,4-Benzodioxan-2-ylcarbonyl)piperazin-1-yl] Derivatives as α_1-Adrenoceptor Antagonists and Antihypertensive Agents. *J. Med. Chem.* **1987**, *30*, 49−57.
(13) Cramer, R. D., III; Patterson, D. E.; Bunce, J. D. Comparative Molecular Field Analysis (CoMFA). 1. Effect of Shape on Binding of Steroids to Carrier Proteins. *J. Am. Chem. Soc.* **1988**, *110*, 5959−5967.
(14) Cramer, R. D., III; DePriest, S. A.; Patterson, D. E.; Hecht, P. The Developing Practice of Comparative Molecular Field Analysis. In *3D QSAR in Drug Design. Theory Methods and Applications*; Kubinyi, H., Ed.; ESCOM Science Publishers: Leiden, 1993; pp 443−485.
(15) Schaper, K.-J.; Emig, P.; Engel, J.; Fleischhauer, I.; Kutscher, B.; Rosado, M. L.; López-Rodríguez, M. L. Dose Response Relationships, Biotest Intercorrelations, QSAR and the Saving of Animals Experiments. *10th European Symposium on Structure-Activity Relationships: QSAR and Molecular Modelling*. Barcelona, 1994.
(16) Cheng, Y. C.; Prusoff, W. H. Relationship between the Inhibition Constant (K_i) and the Concentration of Inhibitor which Causes 50 Per Cent Inhibition (IC_{50}) of an Enzymatic Reaction. *Biochem. Pharmacol.* **1973**, *22*, 3099−3108.
(17) SYBYL 6.0, Tripos Associates, Saint Louis, MO 63144.
(18) Dewar, M. J. S.; Zoebisch, E. G.; Healy, E. F.; Stewart, J. J. P. AM1: A New General Purpose Quantum Mechanical Molecular Model. *J. Am. Chem. Soc.* **1985**, *107*, 3902−3909.
(19) Wold, S.; Albano, C.; Dunn, W. J., III; Edlund, U.; Esbenson, K.; Geladi, P.; Hellberg, S.; Johansson, E.; Lindberg, W.; Sjöström, M. In *Chemometrics: Mathematics and Statistics in Chemistry*; Kowalsky, B. R., Ed.; Reidel: Dordrecht, 1984; pp 17−95.
(20) Dunn, W. J., III; Wold, S.; Edlund, U.; Hellberg, S.; Gasteiger, J. Multivariate Structure-Activity Relationship Between Data from a Battery of Biological Tests and an Ensemble of Structure Descriptors: The PLS Method. *Quant. Struct.-Act. Relat.* **1984**, *3*, 131−137.
(21) Dakin, H. D. Amino Acids of Gelatin. *J. Biol. Chem.* **1920**, *44*, 499−529.
(22) Martin, G. E.; Elgin, R. J., Jr.; Mathiasen, J. R.; Davis, C. B.; Kesslick, J. M.; Baldy, W. J.; Shank, R. P.; DiStefano, D. L.; Fedde, C. L.; Scott, M. K. Activity of Aromatic Substituted Phenylpiperazines Lacking Affinity for Dopamine Binding Sites in a Preclinical Test of Antipsychotic Efficacy. *J. Med. Chem.* **1989**, *32*, 1052−1056.
(23) Clark, R. D.; Weinhardt, K. K.; Berger, J.; Fisher, L. E.; Brown, C. M.; MacKinnon, A. C.; Kilpatrick, A. T.; Spedding, M. 1,9-Alkano-bridged 2,3,4,5-Tetrahydro-1*H*-3-benzazepines with Affinity for the α_2-Adrenoceptor and the 5-HT_{1A} Receptor. *J. Med. Chem.* **1990**, *33*, 633−641.
(24) Ambrosio, E.; Montero, M. T.; Fernández, I.; Azuara, M. C.; Orensanz, L. M. [^{3}H]Prazosin Binding to Central Nervous System Regions of Male and Female Rats. *Neurosci. Lett.* **1984**, *49*, 193−197.

JM960744G